Environmental Science and Pollution Research (2021) 28:3465–3474
https://doi.org/10.1007/s11356-020-10747-7

RESEARCH ARTICLE

Preparation of CuSe-PDA/g-C_3N_4 and its visible-light photocatalytic performance to dye degradation

Maojuan Bai[1] · Chengcheng Xu[1] · Xuanye Huang[1] · Han Yin[1] · Jun Wan[1]

Received: 1 January 2020 / Accepted: 6 September 2020 / Published online: 12 September 2020

Abstract

CuSe as an excellent photocatalytic semiconductor material has wildly used in the field of photocatalysis. In this paper, CuSe-PDA/g-C_3N_4 was designed and synthesized, and the photocatalytic performance of CuSe was further enhanced by the addition of polydopamine (PDA) and graphite phase carbon nitride (g-C_3N_4). The as-prepared CuSe-PDA/g-C_3N_4 was characterized by scanning electron microscope (SEM), transmission electron microscope (TEM), X-ray powder diffraction (XRD), X-ray photoelectron spectroscopy (XPS), Fourier transform infrared spectroscopy (FT-IR), and elemental mapping. The specific surface area and porous characteristics of the material were also studied by N_2 adsorption-desorption isotherm, which the specific surface area were 186.6 m^2/g and pore size were of 3.1 nm by BET data analysis. The photocatalytic conditions for the degradation of methylene blue (MB) by CuSe-PDA/g-C_3N_4 were optimized in the experiment. The results showed that the photocatalytic performance of CuSe-PDA/g-C_3N_4 under visible-light illumination were better than CuSe and PDA owing to the narrow band gap energy and delayed electron-hole recombination. Under the optimized conditions, the removal rate reach to 99% of 50 mg/L MB within 60 min irradiation time. Moreover, the MB removal rate was over 90% through six repeated experiments, which proved that the CuSe-PDA/g-C_3N_4 composite nanomaterials have good stability and reusability.

Keywords Photocatalytic · CuSe · Polydopamine · Graphite phase carbon nitride · Degradation wastewater

Introduction

With the increasingly serious environmental and resource problems, the photocatalysis has aroused widespread concern. Degradation of organic pollutants in the environment or in water by photocatalytic technology is an inexpensive and feasible way to solve the increasingly serious environmental pollution problems. Most of the traditional photocatalytic materials cannot have high visible light utilization rate and high quantum efficiency at the same time, so a new photocatalyst capable of high visible light utilization, high quantum efficiency, high stability, and low cost is prepared, which has become the frontier and hot spot of the current international photocatalysis technology (Steckel et al. 2006; Coe-Sullivan et al. 2005; Chen et al. 2010; Wang et al. 2012).

Copper selenide is a good P-type semiconductor material and can be combined with N-type semiconductor materials to form a PN junction solar cell structure. Copper selenide is a P-type semiconductor with a narrow band gap (Riha et al. 2010; Cao et al. 2007) which is good for better absorption of sunlight and can be used as an excellent photocatalytic material. Dopamine (DA) can facilely self-polymerize to form a film on the surface of inorganic and organic materials, a mussel-inspired stable polydopamine (PDA) layer (Wang et al. 2013). Since the functional groups of PDA including catechol, amines, imines, and quinone, this enables them to bind to a variety of biomolecules without any further surface activation or treatment, which provides a mild and simple way to prepare biofunctionalized nanomaterials. Graphite carbon nitride (g-C_3N_4), a photopolymer containing no polymer metal, has thermal stability, large surface area, and a narrow band gap (Wang et al. 2009; Thomas et al. 2008). Great attention due to its high physicochemical stability, response to visible light, environmentally friendly, and readily available characteristics (Zhu et al. 2015; Wu et al. 2015; Li et al. 2014, 2017). However, the catalytic activity of g-C_3N_4 is still limited due to low quantum efficiency and rapid recombination of photogenerated charges (Jiang and Xie 2016; Zhang et al.

Responsible Editor: Sami Rtimi

✉ Jun Wan
wanjundz@sohu.com

[1] College of Environment and Safety Engineering, Qingdao University of Science and Technology, Qingdao 266042, China

2018). PDAs contain catechol groups whose surface charge can be controlled by protonation and deprotonation (Song et al. 2017; Wang et al. 2019a, b). Thus, a functionalized PDA can be used as an adhesion layer to cure the oppositely charged g-C_3N_4. Crucially, PDA absorption range extends from ultraviolet (UV) light to near-infrared (NIR) areas, giving the PDA excellent light-capturing capabilities (Xie et al. 2016; Mao et al. 2016; Nam et al. 2012).

Hence, smaller CuSe nanomaterials were prepared by deposition, modified with PDA and g-C_3N_4, and composites of CuSe-PDA/g-C_3N_4 were prepared to degrade methylene blue–simulated waste water under visible light irradiation. CuSe and g-C_3N_4 are effectively combined to achieve good adhesion through PDA. PDA as an electron acceptor accelerates the separation and transfer of photogenerated electrons and protons of g-C_3N_4, avoiding electron-hole recombination. g-C_3N_4 has high physical and chemical stability and provides a relatively large specific surface area. By combining the two materials PDA and g-C_3N_4, the adsorption capacity of the composite material is enhanced, the band gap energy of the CuSe sample is reduced, and the energy learned by the electron transition is reduced, thereby enhancing the photocatalytic energy, while CuSe also exhibits a higher affinity for H_2O_2 as a simulated enzyme. The photocatalytic activity of CuSe-PDA/g-C_3N_4 in the presence of H_2O_2 was evaluated by photocatalytic degradation of methylene blue in the presence of visible light.

Materials and methods

Materials and reagents

Selenium powder, $CuSO_4$, Na_2SO_3, 25% ammonia water, melamine, and Tris were purchased from Sinopharm Chemical Reagent Co. Ltd. Dopamine hydrochloride was stocked from Aladdin Industrial Corporation. Other chemical reagents were of analytical grade reagent and required no further refinement. All of the above solutions were prepared using deionized water.

Apparatus

The morphology and microstructure of the samples were observed by SEM and TEM. The crystalline phase of the samples was measured by XRD. XRD instruments are measured using Cu Kα radiation (λ = 1.5406 Å), and the range of 2θ radiation is 20 to 70°. UV spectrophotometer is used to measure the absorbance of the solution. The visible light response characteristics of the samples by UV-visible diffuse reflectance spectroscopy. The chemical composition and chemical structure of the sample can be characterized by XPS and IR. Use BET to detect the specific surface area and pore size of the sample.

Synthesis of CuSe-PDA/g-C_3N_4

On the basis of previous studies, CuSe was prepared by liquid phase coprecipitation (Park et al. 2011; Kumar and Singh 2011; Sonia et al. 2013; Kaviyarasu et al. 2016). Briefly, the Na_2SeSO_3 solution is synthesized by Na_2SO_3 (2.52 g) and selenium powder (0.79 g) at 70 ° C for 3 h in a water bath; ammonia water (25%) was added dropwise to $CuSO_4$ (0.1 mol/L) solution until the solution was clarified to prepare $Cu(NH_3)_4SO_4$. Finally, Na_2SeSO_3 solution and $Cu(NH_3)_4SO_4$ solution were added to the reaction vessel containing L-ethylene glycol, where $Cu(NH_3)_4SO_4$ solution was finally slowly added dropwise. After the addition of the $Cu(NH_3)_4SO_4$ solution, the magnetic stirring at room temperature for 0.5 h, washing with anhydrous ethanol and deionized water for not less than 3 times, and vacuum drying at 60 °C followed.

CuSe-PDA is prepared by chemical coprecipitation (Yu et al. 2017; Li et al. 2019). CuSe (0.5 g) sample was added to 100 mL of water and sonicated for 30 min. Then dopamine hydrochloride (0.5 g) was added and stirred at room temperature for 60 min. Finally, the Tris-HCl buffer (100 mL) was added, adjusted to pH 8.5, and stirred at room temperature for 24 h. The solid was collected, washed three times with deionized water, and vacuum dried at 60 °C.

g-C_3N_4 is prepared by burning method (Qin et al. 2019; Deonikar et al. 2019). Using melamine as raw material, it is fired at 500 °0 in a tube furnace at a heating rate of 5 °i/min for 2 h and is stored after cooling.

CuSe-PDA/g-C_3N_4 is prepared by hydrothermal method (Wang et al. 2018, 2019a, b; He et al. 2019). A certain amount of prepared CuSe-PDA and g-C_3N_4 were added to an autoclave containing 70 mL of water and reacted in an oven at a temperature of 180 °C for 6 h. After cooling to room temperature, it was filtered and washed three times with deionized water and dried under vacuum at 60 °C.

Photocatalytic performance

The photocatalytic performance of the prepared photocatalytic material was evaluated by calculating the photocatalytic degradation rate of the MB solution of the prepared photocatalytic material under dark and visible light conditions. A certain amount of photocatalyst sample was dispersed in 50 ml of MB aqueous solution, and the mixture was stirred under dark conditions for a certain time to achieve an adsorption-desorption equilibrium, and then a 500-W xenon lamp was used as a visible light source, and the suspension was kept under illumination. After centrifugation, the supernatant was taken to measure the absorbance, and the photodegradation efficiency was calculated. The calculation equation is $(1 - C_t/C_0) \times 100\%$. Different photocatalytic conditions were investigated by the following steps. Change a certain factor to

do photocatalysis experiment, get the degradation efficiency at each time by calculation, and draw a graph to compare the influence of this factor on the photocatalysis.

Results and discussions

Morphology and structural characterization

The microscopic and microscopic structures of CuSe, CuSe-PDA, and CuSe-PDA/g-C_3N_4 were shown by SEM and TEM, and the elemental distribution was shown by elemental mapping. As can be seen from Fig. 1a and d, CuSe having a sheet shape is prepared without a regular 2D shape. Self-polymerization of dopamine forms a thin layer of PDA on the periphery of the CuSe nanoflakes, as shown in Fig. 1b and e. In Fig. 1e, it can be seen more clearly that there is a lighter PDA film outside the CuSe nanosheet, and the thickness of the film is about 35 nm. In the figure, CuSe nanosheets were covered by a PDA membrane to form a shell, and no particles without a PDA membrane are observed. It is thus confirmed that PDA thin films are heteroepitaxially grown

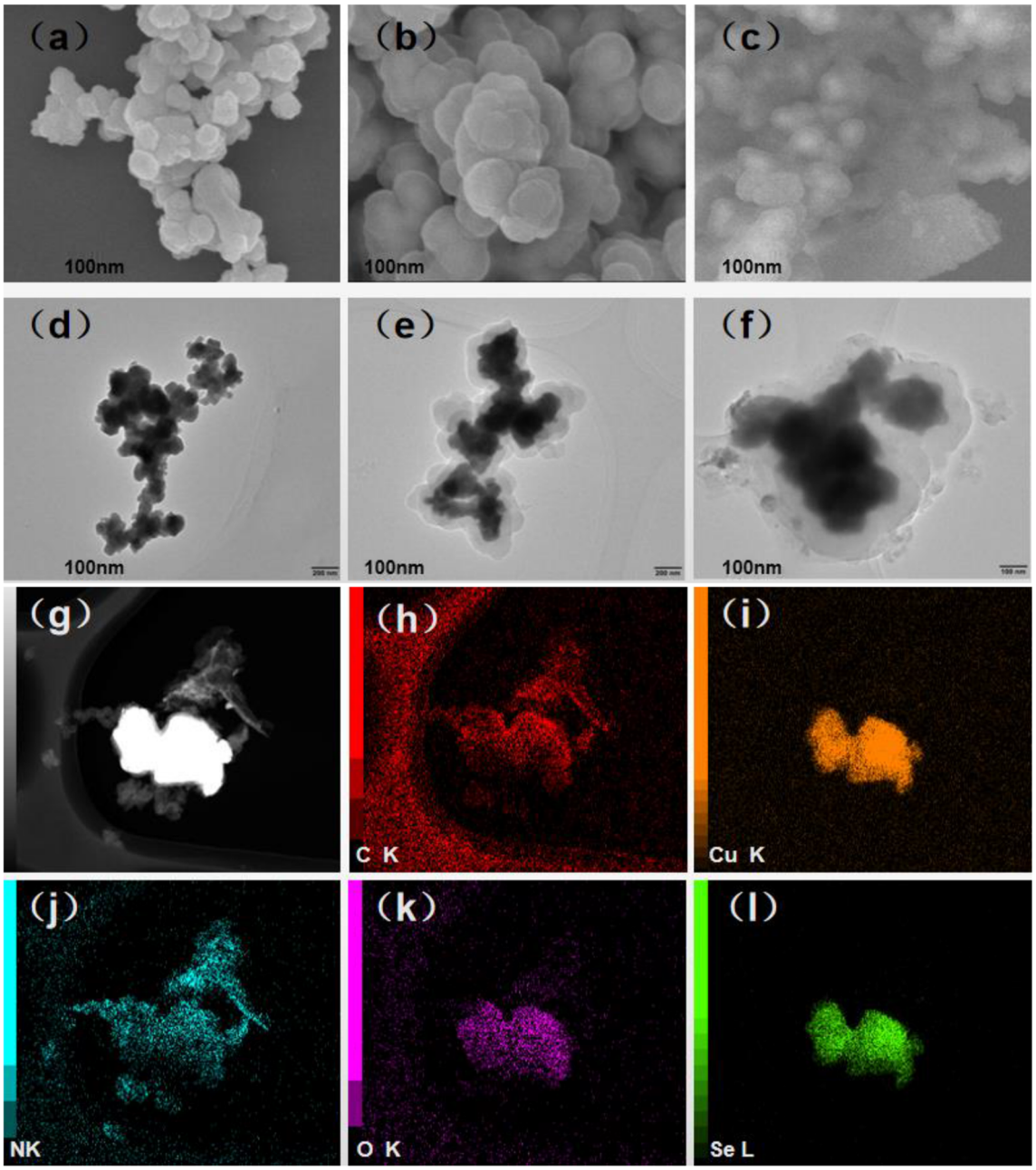

Fig. 1 **a**–**c** SEM images of CuSe, CuSe-PDA, CuSe-PDA/g-C_3N_4; **d**–**f** TEM images of CuSe, CuSe-PDA, CuSe-PDA/g-C_3N_4; **g**–**i** Element distribution picture of CuSe-PDA/g-C_3N_4

on the CuSe nanoflakes, forming the core–shell structure. As shown in Fig. 1c, a CuSe-PDA/g-C_3N_4 carrier was successfully prepared, and sheet-like g-C_3N_4 and CuSe nanoparticles having a PDA film were clearly observed, which is consistent with the SEM image (Fig. 1f). It can be seen from the element distribution of CuSe-PDA/g-C_3N_4 observed in the element map of Fig. 1g–i, Se element and Cu element were located in the inner layer of the sample, and O element evenly distributed on the surface of CuSe shows that PDA and CuSe were tightly bonded. The presence of C and N proves that g-C_3N_4 has been combined with CuSe and PDA. The content of each element in the sample is shown in Table 1, where Cu accounts for 40.75%, Se accounts for 21.15%, C accounts for 32.29%, N accounts for 3.79%, and O accounts for 2.01%. The existence of each element proves that the material is successfully compound.

To further demonstrate the composite of CuSe-PDA/g-C_3N_4, the samples were characterized by XPS, as shown in Fig. 2. The elements of XPS reaction are consistent with the elements reflected by EDS, and all contain Cu, Se, C, N, and O, which can further prove that CuSe is successfully in accordance with PDA and g-C_3N_4. In the survey XPS spectrum (Fig. 2a) of CuSe-PDA/g-C_3N_4, we can see peaks corresponding to N 1s (399 eV), O 1s (531.8 eV), Cu 2p (931.8 eV), Se 3d (53.15), and C 1s (284.8 eV). The peak at 284.8 eV is mainly caused by the extrapolated carbon on the surface of the material. Figure 2b shows the spectrum of N1s was analyzed at the binding energy of 398.8 eV. The binding energy peak here indicates that the N element is present in the sample. Sp^2-hybridized aromatic N bonded to carbon atoms (C=N–C) caused the peak of 398.5 eV. The peak of the binding energy of 399.2 eV indicates the role of the tertiary N bonded to carbon atoms in the form of N–C_3. Another peak at 400.7 eV is attributed to the amino groups (C–N–H_2). Figure 2c also shows that the three binding energy peaks are 284.5 eV, 285.5 eV, and 288.1 eV. The peak of binding energy at 284.5 eV is due to the –C–C group, a peak at 285.5 eV, which corresponds to C–O and C=N, and a peak at 288.1 eV, which is assigned to N–C_3. The spectrum of O 1s was analyzed at 532 eV, demonstrating the presence of PDA in the sample. Figure 2d shows the two binding energy peaks of O 1s. The characteristic peaks at these two points correspond to C–O (531 eV) and C=O (531.4 eV). In Fig. 2e–f, the peaks of 931.8 eV and 951.9 eV react with the binding energy of Cu2p3/2 and Cu2p1/2, and the peak of 54.5 eV reflects the binding energy of Se3d, which proves the existence of CuSe in the material. In summary, the XPS spectrum of the sample indicates that PDA and g-C_3N_4 were successfully compounded in the sample.

Table 1 Proportion elements of CuSe-PDA/g-C_3N_4 by EDS

Element	C	N	O	Cu	Se
Mass%	32.29	3.79	2.01	40.75	21.15

The infrared spectrum of Fig. 3 depicts the chemical structure of CuSe-PDA/g-C_3N_4 similar to the graphite structure. And Fig. 3 also shows the infrared spectrum of PDA and g-C_3N_4. The peak at 810 cm^{-1} is designated as s-triazine ring mode (Sonia et al. 2013). The broad peak at 1254–1632 cm^{-1} is due to the tensile vibration of C–NH–C and N–(C)3, which proves the existence of g-C_3N_4. The stretching vibration modes of CH and CH2 determined two peaks at 2917 cm^{-1} and 2852 cm^{-1}. The peak appearing at 3442 cm^{-1} is mainly caused by the stretching vibration of the N–H and O–H bonds, which proved that the PDA was successfully introduced into the sample.

The crystal phase of CuSe is characterized using an X-ray diffraction and the XRD diffraction pattern was shown in Fig. 4a. The sample have five peaks at the 2θ values of 26.6°, 31.1°, 44.6°, 52.9°, and 65.9° corresponding to the (111), (200), (220), (311), and (400) planes. The diffraction peak of the prepared nanosheet is directed to CuSe by comparison with a standard card with the lattice constants α = 1.5406 Å, which are fits well with the standard JCPDS card No.06-0680. By comparison with the standard card, other impurity peaks were not found, which proved that prepared CuSe was pure phase. Figure 4b shows the XRD image of pure g-C_3N_4 with a characteristic peak of g-C_3N_4 at (002) (Yu et al. 2017), which is also reflected in Fig. 4c. Figure 4c shows the XRD pattern of CuSe-PDA/g-C_3N_4, which contains the characteristic peak of CuSe, the strong peak of C_3N_4 (002), and some other weak peaks, indicating that CuSe-PDA/g-C_3N_4 is effectively combined.

Optical properties of the materials

Figure 5 are two graph showing the visible light response characteristics of CuSe, CuSe-PDA, and CuSe-PDA/g-C_3N_4 by UV-visible diffuse reflectance spectroscopy. It can be seen from Fig. 5a that the absorption spectra of CuSe and CuSe-PDA are similar, and CuSe-PDA/g-C_3N_4 is quite different from the two. The absorption edges of CuSe and CuSe-PDA are similar, which are 432 nm and 450 nm, indicating that the UV activity of the two is relatively large. The absorption edge of CuSe-PDA/g-C_3N_4 reaches 652 nm, which not only compensates for the absorption of the ultraviolet region, but also has a good response to the visible region. The forbidden band width can be calculated by plotting the hv (vs) ahv map, the equation is $(ahv)^{1/n} = K(hv - Eg)$, where n = 1/2 is the direct band gap and n = 2 is the indirect band gap (Niu et al. 2012). CuSe is a direct band gap semiconductor, and the relationship between $(ah_v)^2$ and h_v is shown in Fig. 5b. The band gap energies of CuSe, CuSe-PDA, and CuSe-PDA/g-C_3N_4 can

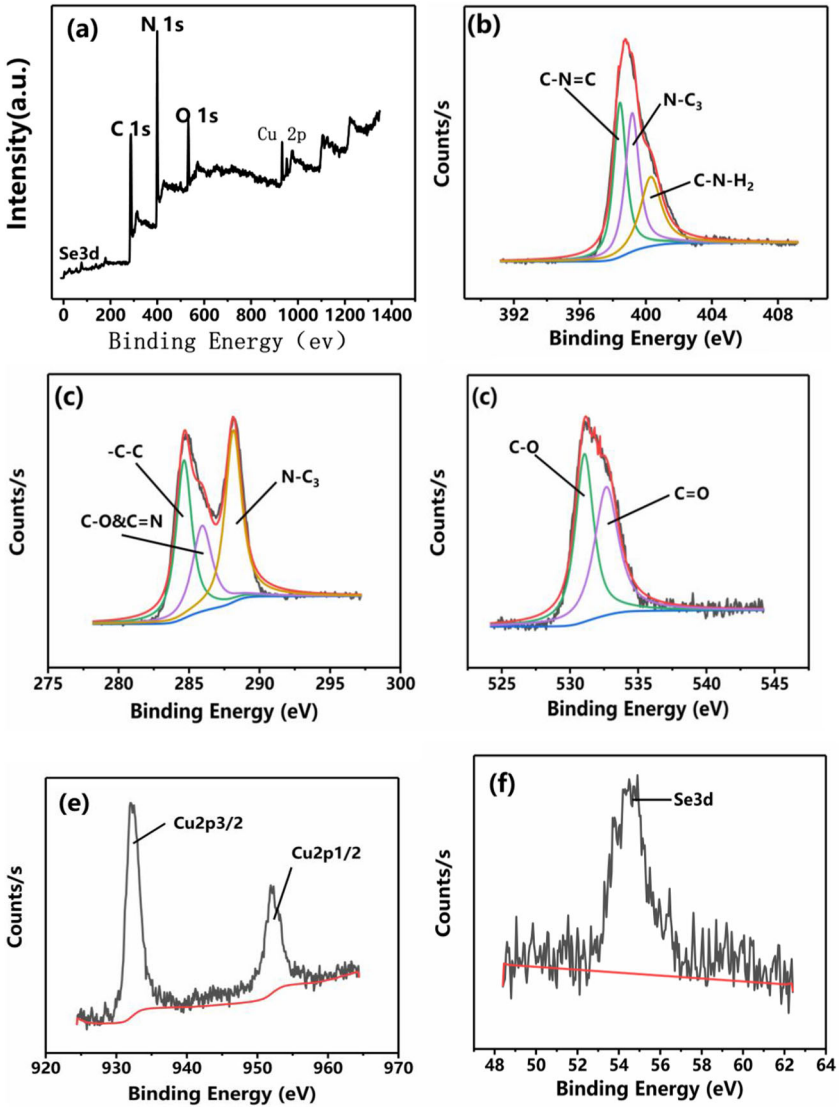

Fig. 2 **a**–**f** XPS survey spectra of CuSe-PDA/g-C_3N_4

be estimated to be 2.9 eV, 2.8 eV, and 1.8 eV, respectively. This proves that CuSe becomes smaller in band gap after compositing with PDA and g-C_3N_4, and the photocatalytic effect is enhanced.

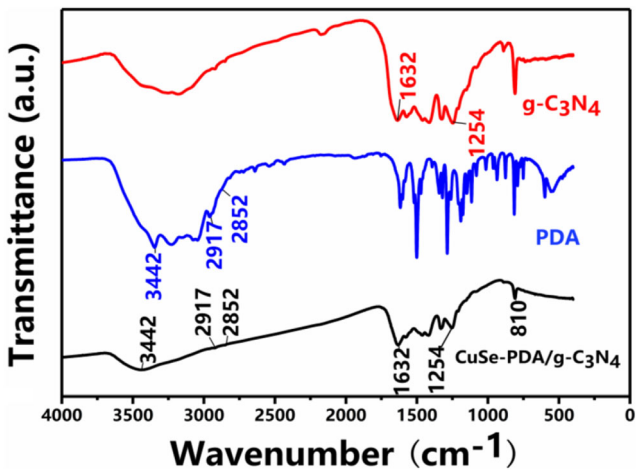

Fig. 3 FTIR spectra of g-C_3N_4, PDA, and CuSe-PDA/g-C_3N_4

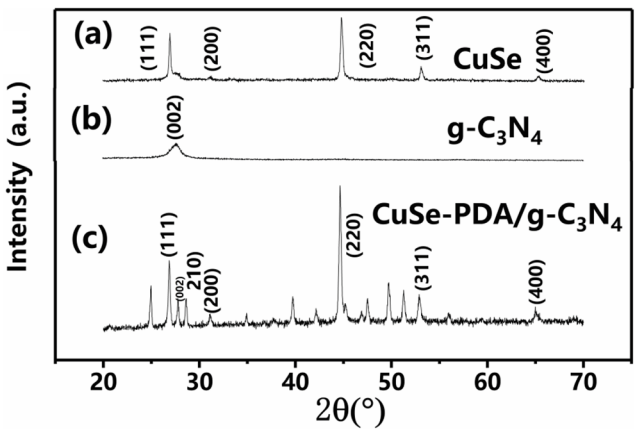

Fig. 4 XRD patterns of CuSe and CuSe-PDA/g-C_3N_4

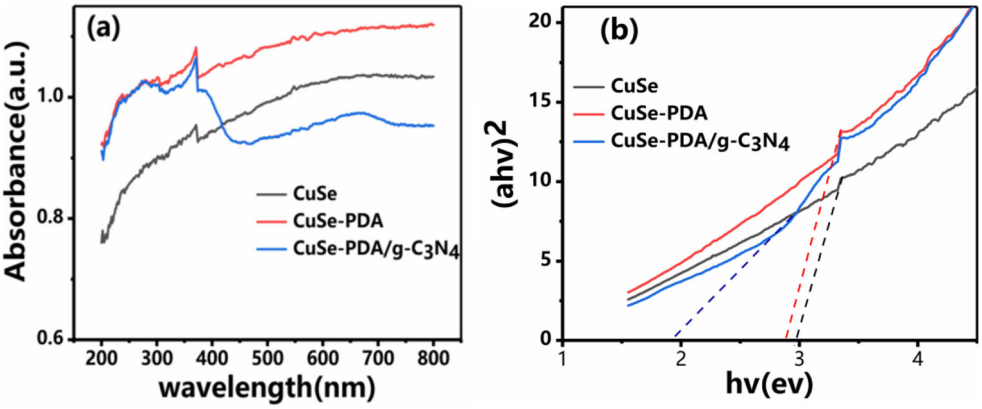

Fig. 5 UV–vis spectrum (a) and estimated band gap (b) of CuSe, CuSe-PDA and CuSe-PDA/g-C_3N_4

Material adsorption characteristics

The specific surface area and porous characteristics of the material were studied by N_2 adsorption-desorption isotherm. The N_2 adsorption-desorption isotherms and their pore size distribution of CuSe-PDA/g-C_3N_4 samples are shown in Fig. 6a. The specific surface area and pore size of the material obtained by BET data analysis, which were 186.6 m^2/g and 3.1 nm. According to the classification of IUPAC (Meng et al. 2015), the sample isotherm belongs to the type IV curve with H_2 hysteresis loop type. At a lower relative pressure, the amount of adsorption rises rapidly, the curve is convex, and the isotherm has an inflection point, explain that single layer adsorption reaches saturation. Under medium relative pressure, the isotherm of the capillary condensation phenomenon continues to rise, and the adsorption hysteresis loop appears near the isotherm 0.4–0.8, which proves that the material has a rich mesoporous structure. It can be seen from Fig. 6b that the material pore size is uniformly distributed around 2–5 nm, which is the same as the measured result.

Photocatalytic condition optimization

A suitable MB concentration was selected in the experiment to screen the appropriate solution volume ratio of Na_2SeSO_3 solution to $Cu(NH_3)_4SO_4$ solution. As can be seen from Fig. 7a, compared with other solution volume ratios, the ratio of 3:1 is the best, so CuSe is prepared to optimize the solution volume ratio is 3:1. The reason for this is that when the Se element is excessive, it can fully combine with the Cu element, but when the amount of the Se element is too large, the photocatalytic effect is not obvious.

The photocatalytic properties of CuSe, CuSe-PDA, and CuSe-PDA/g-C_3N_4 samples were determined under dark and visible light conditions. Figure 7b shows that the degradation performance of different photocatalysts decreases with the order of CuSe-PDA/g-C_3N_4 > CuSe-PDA > CuSe. The addition of PDA improves the adsorption capacity of photocatalytic materials with the improvement of degradation ability, and then adds g-C_3N_4 to provide a larger specific surface area, which improves the degradation rate. Therefore, CuSe-PDA/g-C_3N_4 samples will end up degrading in about 20 min, while CuSe-PDA takes more than twice as long to end. Therefore, CuSe-PDA/g-C_3N_4 samples have higher photocatalytic activity.

Figure 7c shows the comparison of photocatalytic activity of different molar ratios of CuSe-PDA and g-C_3N_4. It is obvious that the degradation performance decreases with the order of 1:1 > 2:1 > 1:2, 1:1 ratio light effect is the best. The three ratios have almost the same adsorption effect in the dark, indicating that the change of the ratio does not affect the adsorption capacity. The reason may be that the PDA content

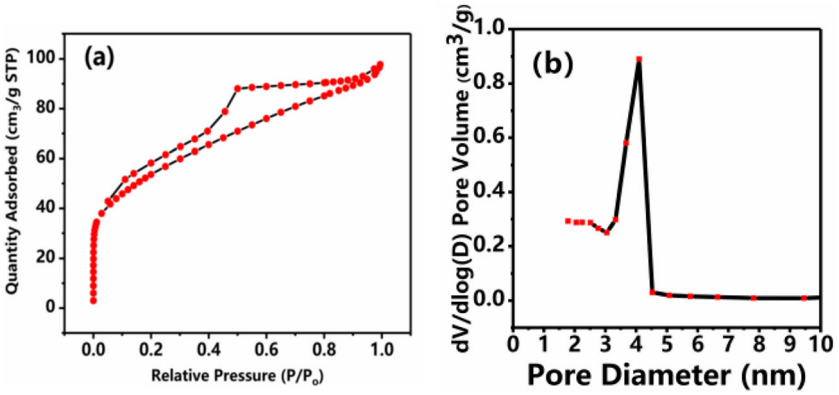

Fig. 6 Nitrogen adsorption-desorption isotherm (**a**) and corresponding BJH pore size distribution curve (**b**) of CuSe-PDA/g-C_3N_4 samples

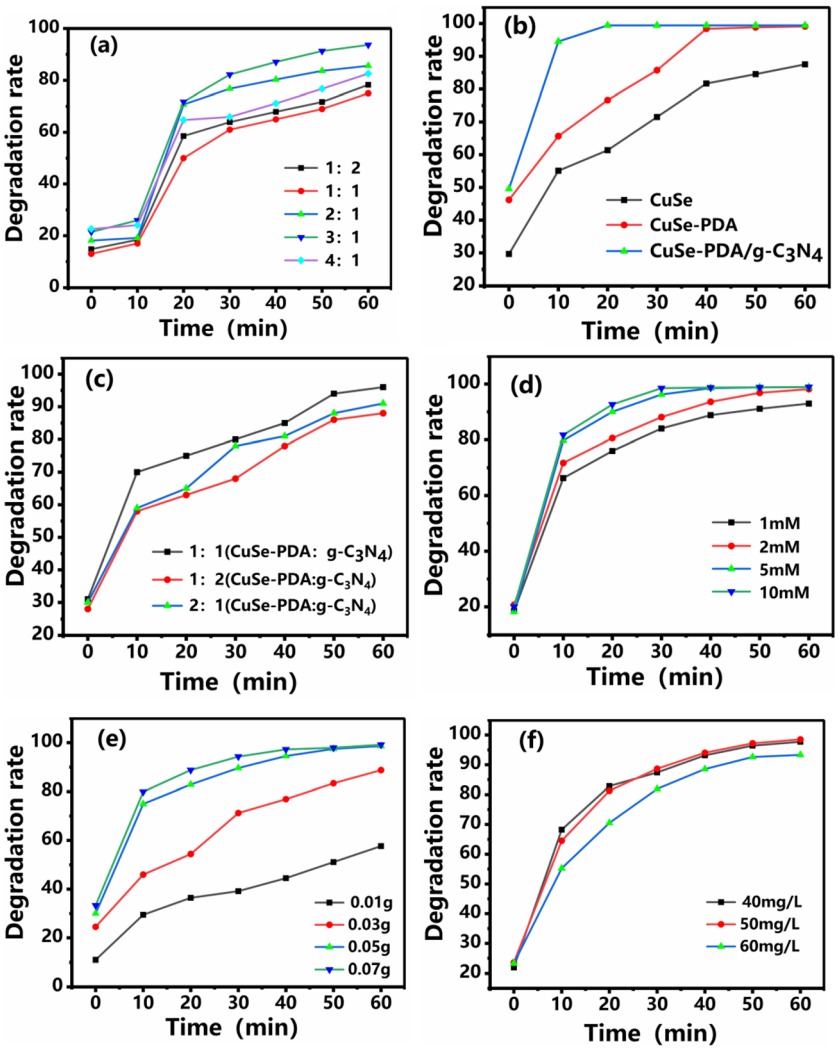

Fig. 7 Optimized the photocatalytic condition: different molar ratio of Na_2SeSO_3 and $Cu(NH_3)_4SO_4$ solution (**a**), the effect of three photocatalysts to MB (**b**), the proportion of CuSe-PDA and g-C_3N_4 (**c**), concentration of H_2O_2 (**d**), dosage of photocatalysts (**e**), the effect of MB concentration (**f**)

has reached the optimum and cannot further enhance the adsorption capacity of the composite. An increase in the content of g-C_3N_4 may hinder the light from reaching the active site of the semiconductor material, so the result is reasonable; the molar ratio of 1:2 has the worst photocatalytic effect compared with the other two molar ratios.

H_2O_2 plays an important role in photocatalytic degradation of MB. It can be seen from Fig. 7d that with the increase of H_2O_2 concentration, the catalytic rate of CuSe-PDA/g-C_3N_4 is gradually increased. The addition of H_2O_2 can promote the production of OH, thereby enhancing the degradation of MB (Gao et al. 2016). However, the final catalytic effects of 2

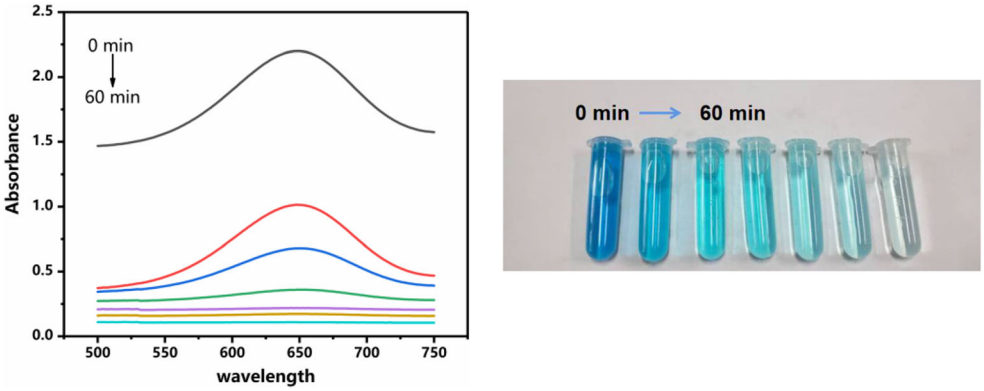

Fig. 8 CuSe-PDA/g-C_3N_4 degradation MB digital photo and ultraviolet absorption curve

Table 2 Degradation rate of other materials

Material	Concentration	Degradation rate	Literature
TiO_2	20 mg/L	76	Ghosh et al. 2020
PDA/RGO/Ag_3PO_4/PVDF	20 mg/L	99%	Zhang et al. 2019
Ag_2O/g-C_3N_4	10 mg/L	100%	Liang et al. 2019
g-C_3N_4/ZnO	10 mg/L	98%	Zhong et al. 2020
CuSe-PDA/g-C_3N_4	50 mg/L	97%	This work

mM, 5 mM, and 10 mM concentrations are almost the same, so from the economic point of view, 2 mM H_2O_2 is the optimal concentration.

Figure 7e is a photodegradation curve for the amount of different CuSe-PDA/g-C_3N_4 catalysts. It can be seen from the figure that the degradation rate of MB becomes larger as the amount of catalyst increases. When the dosage is 0.05 g and 0.07 g, the degradation rate of MB reaches the maximum, which is 96.6% and 97.0%. The catalytic effects of the two are almost the same. When the amount of catalyst is small, the amount of organic molecules adsorbed per unit time is relatively small, resulting in a slower degradation rate of MB, and the final degradation effect is not good. When the amount of the catalyst is too large, the catalyst may be piled up, thereby reducing the absorption ability of light, and it may also cause a part of the overlapping catalysts to fail to absorb light to perform photocatalysis. Therefore, from the perspective of economy and practicality, choose 0.05 g as the best dosage.

Figure 7f shows the effect of different initial concentrations of MB on the photocatalytic degradation. It can be seen from the figure that when the initial concentration of MB is small, it has a higher reaction rate in the initial stage, and the final removal rate is also higher. When the initial concentration of MB is large, not only the initial rate of degradation is slow, but also the final degradation rate is low. Because the solution concentration of MB per unit time far exceeds the degradation ability of the catalyst for the catalyst, and the excessive initial concentration does not increase the adsorption amount of the catalyst. At the same time, the excess MB solution also provides greater chromaticity, and the irradiation of light is hindered, so that the degradation efficiency is lowered, and the final degradation rate is not satisfactory. The highest concentration of the catalyst that can be achieved in the figure is 50 mg/L, so the optimal initial concentration of MB for the experiment is 50 mg/L.

The digital picture and UV absorption curve of the MB degradation of CuSe-PDA/g-C3N4 material within 60 min are shown in Fig. 8.The degradation rate is the fastest within 0 to 10 min, and the color change is the most obvious.

The degradation rate of other materials is shown in Table 2. As the earliest photocatalytic material, TiO2 only has a degradation rate of 76% when processing 20 mg/L of methylene blue dye, which is inferior to other materials. CuSe-PDA/g-C_3N_4 material can degrade MB of 50 mg/L to 97%, which has stronger photocatalytic performance than other materials.

The reaction mechanism of CuSe-PDA/g-C_3N_4 degraded MB

Figure 9 shows the basic mechanism of CuSe-PDA/g-C_3N_4 material degradation of pollutants in water. First, under the irradiation of light, the material is excited by photons with energy greater than or equal to its forbidden band width to generate photo-generated electrons (e^-) and holes (h^+) with a certain energy; transfer or deactivation of photogenerated electrons (e^-) and holes (h^+) inside and between materials; the photogenerated electrons (e^-) and holes (h^+) reach the surface of the material and interact with the substances on the surface or the substances in the solvent, that is, the redox reaction occurs, thereby generating some radical groups with strong oxidizing properties (·OH, O_2^-); the strong oxidizing free radicals and oxidizing substances generated above fully interact with the degraded pollutants, causing them to oxidize or degrade into carbon dioxide and water (Chong et al. 2010; Chen et al. 2019). H_2O_2 is also added during the reaction. It can decompose in the aqueous solution to generate a small amount of hydroxyl radicals, which can destroy the molecular structure of MB and cause it to decompose into small molecular inorganic substances (Mi et al. 2013; Xue et al. 2019). Moreover, CuSe has peroxidase-like properties, which can promote the hydrolysis of H_2O_2 to produce strong oxidizing

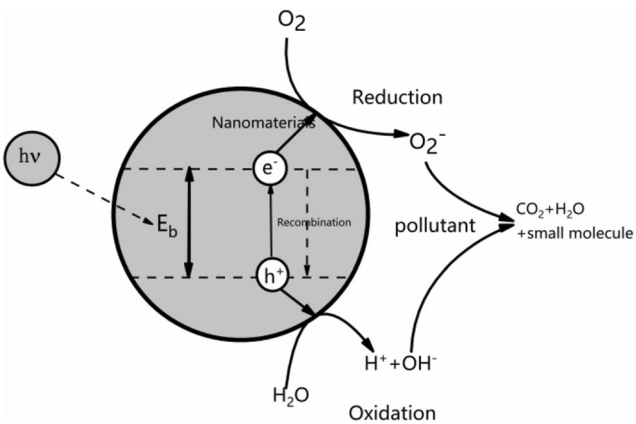

Fig. 9 Mechanism of photocatalytic degradation of water pollutants

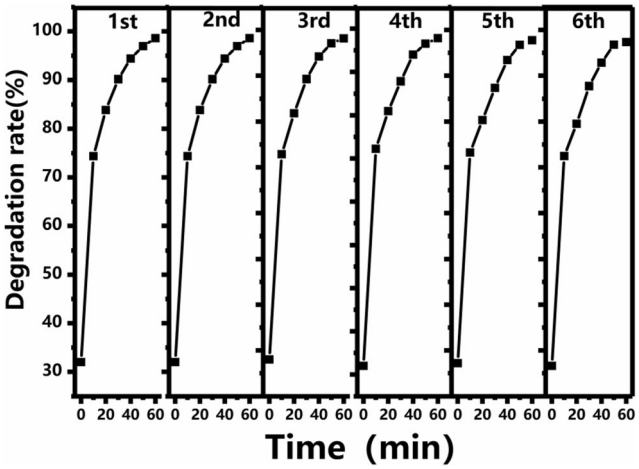

Fig. 10 Recycling test of CuSe-PDA/g-C_3N_4 under visible light irradiation

groups such as OH^- and·OH, and the degradation of pollutants is further accelerated.

Repeat experiment

Figure 10 shows repeated experiment of photodegradation of MB 6 times under the same conditions. Each experiment was carried out under the optimal conditions of an initial concentration of 50 mg/L MB, a CuSe-PDA/g-C_3N_4 catalyst dosage of 0.05 g, a H_2O_2 concentration of 2 mM, and an optical power of 500 W. After 6 repeated experiments, the degradation rate of MB was still greater than 90%, indicating that CuSe-PDA/g-C_3N_4 catalyst has good stability and reusability.

Conclusion

CuSe and CuSe-PDA were prepared by liquid phase coprecipitation method, and CuSe-PDA/g-C_3N_4 composite was prepared by hydrothermal method. The morphology, structure, and properties were characterized by SEM, TEM, XRD, XPS, FTIR, and element distribution mapping. Compared with CuSe and CuSe-PDA, CuSe-PDA/g-C_3N_4 composite exhibited excellent photocatalytic degradation of MB under visible light irradiation and attributed to the superior adsorption performance, excellent electrical conductivity, and efficient transport of g-C_3N_4 and PDA. And the specific surface area of nanocomposite was of 186.6 m^2/g, and pore size was 3.1 nm by BET data analysis, while CuSe with the characteristic of simulating enzyme can be used in AOPs for organic pollutants. In addition, the MB removal rate was over 90% through six repeated experiments, which proved that the CuSe-PDA/g-C_3N_4 composite samples have good stability and reusability.

Funding This work was supported by the Natural Science Foundation of Shandong Province (ZR2017MB049).

Compliance with ethical standards

Conflict of interest The authors declare that they have no conflict of interest.

References

Cao H, Gong Q, Qian X, Wang H, Zai J, Zhu Z (2007) Synthesis of 3-D hierarchical dendrites of lead chalcogenides in large scale via microwave-assistant method. Cryst Growth Des 7(2):425–429

Chen X, Shen S, Guo L, Mao SS (2010) Semiconductor-based photocatalytic hydrogen generation. Chem Rev 110(11):6503–6570

Chen J, He Z, Ji Y, Li G, An T, Choi W (2019) OH radicals determined photocatalytic degradation mechanisms of gaseous styrene in TiO_2 system under 254 nm versus 185 nm irradiation: Combined experimental and theoretical studies. Appl Catal B Environ 257:117912

Chong MN, Jin B, Chow CW, Saint C (2010) Recent developments in photocatalytic water treatment technology: a review. Water Res 44(10):2997–3027

Coe-Sullivan S, Steckel JS, Kim L, Bawendi MG, Bulovic V (2005) Method for fabrication of saturated RGB quantum dot light-emitting devices. In Light-Emitting Diodes: Research, Manufacturing, and Applications IX (Vol. 5739, pp. 108-115)

Deonikar VG, Reddy KK, Chung WJ, Kim H (2019) Facile synthesis of Ag_3PO_4/g-C_3N_4 composites in various solvent systems with tuned morphologies and their efficient photocatalytic activity for multi-dye degradation. J Photochem Photobiol A Chem 368:168–181

Gao F, Zhu L, Wang Y, Xie H, Li J (2016) Room temperature facile synthesis of Cu_2Se hexagonal nanoplates array film and its high photodegradation activity to methyl blue with the assistance of H_2O_2. Mater Lett 183:425–428

Ghosh M, Mondal M, Mandal S, Roy A, Chakrabarty S, Chakrabarti G, Pradhan SK (2020) Enhanced photocatalytic and antibacterial activities of mechanosynthesized TiO_2-Ag nanocomposite in wastewater treatment. J Mol Struct 1211:128076

He W, Tao B, Yang Z, Yang G, Guo X, Liu PJ, Yan QL (2019) Mussel-inspired polydopamine-directed crystal growth of core-shell n-Al@ PDA@ CuO metastable intermixed composites. Chem Eng J 369: 1093–1101

Jiang Z, Xie J (2016) In situ growth of Ag/Ag_2O nanoparticles on g-C_3N_4 by a natural carbon nanodot-assisted green method for synergistic photocatalytic activity. RSC Adv 6(4):3186–3197

Kaviyarasu K, Ayeshamariam A, Manikandan E, Kennedy J, Ladchumananandasivam R, Gomes UU, Maaza M (2016) Solution processing of CuSe quantum dots: photocatalytic activity under RhB for UV and visible-light solar irradiation. Mater Sci Eng B 210:1–9

Kumar P, Singh K (2011) Synthesis, characterizations, and optical properties of copper selenide quantum dots. Struct Chem 22(1):103–110

Li H, Liu J, Hou W, Du N, Zhang R, Tao X (2014) Synthesis and characterization of g-C_3N_4/Bi_2MoO_6 heterojunctions with enhanced visible light photocatalytic activity. Appl Catal B Environ 160:89–97

Li J, Hao H, Zhou J, Li W, Lei N, Guo L (2017) Ag@ AgCl QDs decorated g-C_3N_4 nanoplates: The photoinduced charge transfer behavior under visible light and full arc irradiation. Appl Surf Sci 422(15):626–637

Li L, Zhong D, Xu Y, Zhong N (2019) A novel superparamagnetic micro-nano-bio-adsorbent PDA/Fe_3O_4/BC for removal of hexavalent

chromium ions from simulated and electroplating wastewater. Environ Sci Pollut Res:1–13

Liang S, Zhang D, Pu X, Yao X, Han R, Yin J, Ren X (2019) A novel Ag_2O/g-C_3N_4 p-n heterojunction photocatalysts with enhanced visible and near-infrared light activity. Sep Purif Technol:786–797

Mao WX, Lin XJ, Zhang W, Chi ZX, Lyu RW, Cao AM, Wan LJ (2016) Core–shell structured TiO_2@ polydopamine for highly active visible-light photocatalysis. Chem Commun 52(44):7122–7125

Meng S, Ning X, Zhang T, Chen SF, Fu X (2015) What is the transfer mechanism of photogenerated carriers for the nanocomposite photocatalyst Ag_3PO_4/g-C_3N_4, band–band transfer or a direct Z-scheme. Phys Chem Chem Phys 17(17):11577–11585

Mi L, Li Z, Chen W, Ding Q, Chen Y, Zhang Y, Zheng Z (2013) 3D $Cu_{2-x}Se$ nano/micropeony architectures: large-scale solvothermal synthesis, characterization, and catalytic properties. Thin Solid Films 534:22–27

Nam HJ, Kim B, Ko MJ, Jin M, Kim JM, Jung DY (2012) A new mussel-inspired polydopamine sensitizer for dye-sensitized solar cells: controlled synthesis and charge transfer. Chem Eur J 18(44):14000–14007

Niu P, Zhang L, Liu G, Cheng HM (2012) Graphene-like carbon nitride nanosheets for improved photocatalytic activities. Adv Funct Mater 22(22):4763–4770

Park YS, Okamoto Y, Kaji N, Tokeshi M, Baba Y (2011) Aqueous phase-synthesized small CdSe quantum dots: adsorption layer structure and strong band-edge and surface trap emission. J Nanopart Res 13(11):5781–5798

Qin L, Huang D, Xu P, Zeng G, Lai C, Fu Y et al (2019) In-situ deposition of gold nanoparticles onto polydopamine-decorated g-C_3N_4 for highly efficient reduction of nitroaromatics in environmental water purification. J Colloid Interface Sci 534:357–369

Riha SC, Johnson DC, Prieto AL (2010) Cu_2Se nanoparticles with tunable electronic properties due to a controlled solid-state phase transition driven by copper oxidation and cationic conduction. J Am Chem Soc 133(5):1383–1390

Song XR, Li SH, Dai J, Song L, Huang G, Lin R, Yang HH (2017) Polyphenol-inspired facile construction of smart assemblies for ATP-and pH-responsive tumor MR/optical imaging and photothermal therapy. Small 13(20):1603997

Sonia S, Kumar PS, Mangalaraj D, Ponpandian N, Viswanathan C (2013) Influence of growth and photocatalytic properties of copper selenide (CuSe) nanoparticles using reflux condensation method. Appl Surf Sci 283:802–807

Steckel JS, Snee P, Coe-Sullivan S, Zimmer JP, Halpert JE, Anikeeva P, Kim LA, Bulovic V, Bawendi MG (2006) Color-saturated green-emitting QD-LEDs. Angew Chem Int Ed 45(35):5796–5799

Thomas A, Fischer A, Goettmann F, Antonietti M, Müller JO, Schlögl R, Carlsson JM (2008) Graphitic carbon nitride materials: variation of structure and morphology and their use as metal-free catalysts. J Mater Chem 18(41):4893–4908

Wang X, Maeda K, Thomas A, Takanabe K, Xin G, Carlsson JM, Antonietti M (2009) A metal-free polymeric photocatalyst for hydrogen production from water under visible light. Nat Mater 8(1):76–80

Wang X, Blechert S, Antonietti M (2012) Polymeric graphitic carbon nitride for heterogeneous photocatalysis. ACS Catal 2(8):1596–1606

Wang W, Li R, Tian M, Liu L, Zou H, Zhao X, Zhang L (2013) Surface silverized meta-aramid fibers prepared by bio-inspired poly (dopamine) functionalization. ACS Appl Mater Interfaces 5(6):2062–2069

Wang J, Li M, Zhou S, Xue A, Zhang Y, Zhao Y, Zhong J (2018) Controllable construction of polymer/inorganic interface for poly (vinyl alcohol)/graphitic carbon nitride hybrid pervaporation membranes. Chem Eng Sci 181:237–250

Wang H, Lin Q, Yin L, Yang Y, Qiu Y, Lu C, Yang H (2019a) Biomimetic design of hollow flower-like g-C_3N_4@ PDA organic framework nanospheres for realizing an efficient photoreactivity. Small 15(16):1900011

Wang Q, Peng L, Gong Y, Jia, FLi, Y. (2019b) Mussel-inspired Fe_3O_4@ Polydopamine (PDA)-MoS_2 core–shell nan., Song, S., & osphere as a promising adsorbent for removal of Pb^{2+} from water. J Mol Liq 282:598–605

Wu M, Yan JM, Zhang XW, Zhao M, Jiang Q (2015) Ag_2O modified g-C_3N_4 for highly efficient photocatalytic hydrogen generation under visible light irradiation. J Mater Chem A 3(30):15710–15714

Xie A, Zhang K, Wu F, Wang N, Wang Y, Wang M (2016) Polydopamine nanofilms as visible light-harvesting interfaces for palladium nanocrystal catalyzed coupling reactions. Catal Sci Technol 6(6):1764–1771

Xue F, Si Y, Wang M, Liu M, Guo L (2019) Toward efficient photocatalytic pure water splitting for simultaneous H_2 and H_2O_2 production. Nano Energy 62:823–831

Yu Z, Li F, Yang Q, Shi H, Chen Q, Xu M (2017) Nature-mimic method to fabricate polydopamine/graphitic carbon nitride for enhancing photocatalytic degradation performance. ACS Sustain Chem Eng 5(9):7840–7850

Zhang S, Gao H, Huang Y, Wang X, Hayat T, Li J, Wang X (2018) Ultrathin g-C_3N_4 nanosheets coupled with amorphous Cu-doped FeOOH nanoclusters as 2D/0D heterogeneous catalysts for water remediation. Environ Sci Nano 5(5):1179–1190

Zhang R, Cai Y, Zhu X, Han Q, Zhang T, Liu Y et al (2019) A novel photocatalytic membrane decorated with PDA/RGO/Ag_3PO_4 for catalytic dye decomposition. Colloids Surf A Physicochem Eng Asp:68–76

Zhong Q, Lan H, Zhang M, Zhu H, Bu M (2020) Preparation of heterostructure g-C_3N_4/ZnO nanorods for high photocatalytic activity on different pollutants (MB, RhB, Cr(VI) and eosin). Ceram Int

Zhu T, Song Y, Ji H, Xu Y, Song Y, Xia J, Li H (2015) Synthesis of g-C_3N_4/Ag_3VO_4 composites with enhanced photocatalytic activity under visible light irradiation. Chem Eng J 271:96–105